

THESIS FOR LICENTIATE OF ENGINEERING IN THERMO AND FLUID  
DYNAMICS

Drag Reduction by means of Active Flow Control Applied on  
a Generic Truck A-pillar: a Numerical and Experimental  
Study

GUGLIELMO MINELLI

Department of Applied Mechanics  
CHALMERS UNIVERSITY OF TECHNOLOGY

Gothenburg, Sweden 2016

Drag Reduction by means of Active Flow Control Applied on a Generic Truck A-pillar: a  
Numerical and Experimental Study  
GUGLIELMO MINELLI

© GUGLIELMO MINELLI, 2016

THESIS FOR LICENTIATE OF ENGINEERING no 2016:12

ISSN 1652-8565

Department of Applied Mechanics

Chalmers University of Technology

SE-412 96 Gothenburg

Sweden

Telephone: +46 (0)31-772 1000

Chalmers Reproservice  
Gothenburg, Sweden 2016

Drag Reduction by means of Active Flow Control Applied on a Generic Truck A-pillar: a Numerical and Experimental Study  
THESIS FOR LICENTIATE OF ENGINEERING in Thermo and Fluid Dynamics  
GUGLIELMO MINELLI  
Department of Applied Mechanics  
Chalmers University of Technology

## ABSTRACT

The overall goal of this thesis is to isolate and control the flow mechanism characterizing the flow separation occurring at the A-pillar of a truck. The study aims to gain knowledge of the flow physics of the separation mechanism, and to eventually suppress the aforementioned separation by means of an Active Flow Control.

State of the art unsteady numerical simulations and experiments are both employed to carry out this work. LES are performed at  $Re = 1 \times 10^5$  and post processed (by means of POD and FFT), to study the physics of the flow structures. Further, the hybrid PANS method is tested on several bluff body flows evaluating limits and qualities. The use of a hybrid technique as such is necessary to minimize the computer resources, while still being able to simulate a "close to reality"  $Re$ . In the last part of the work, PANS are validated against wind tunnel experiments on a 3-D generic truck cabin. In the latter part PANS simulations are also employed to conduct an optimization study of the actuation frequency.

Keywords: Vehicle Aerodynamic, Bluff Body Flow, Active Flow Control, AFC, Modal Decomposition, POD, Large Eddy Simulation, LES, Partially Averaged Navier Stokes, PANS, Experiments, Wind Tunnel.



## LIST OF PUBLICATIONS

This thesis is based on the work contained in the following publications:

- Paper A** G. Minelli, S. Krajnović, B. Basara, B. R. Noack, "Numerical investigation of active flow control around a generic truck A-pillar" in *Flow, Turbulence and Combustion*. Paper under review.
- Paper B** S. Krajnović, G. Minelli, B. Basara "Partially-Averaged Navier-Stokes Simulations of two bluff body flows" in *Applied Mathematics and computation* Vol. 000, pp 1-15, 2015
- Paper C** S. Krajnović, G. Minelli, B. Basara "Partially-Averaged Navier-Stokes Simulations of Flows Around Generic Vehicle at Yaw" in *SAE Technical Paper* 2016-01-1586, 2016, doi:10.4271/2016-01-1586
- Paper D** G. Minelli, E. Adi Hartono, S. Krajnović, V. Chernoray, L. Hjelm, B. Basara, "Experimental and Numerical Investigation of Active Flow Control on a Generic Truck Cabin" in *11th International ERCOFTAC Symposium on Engineering Turbulence Modelling and Measurements*, September 21-23, 2016, Palermo, Italy. Paper submitted.

Other publications related to the thesis by the author:

- Publication 1** S. Krajnović, G. Minelli, "Status of PANS for bluff body aerodynamics of engineering relevance" in *Notes on Numerical Fluid Mechanics and Multidisciplinary Design*, 130 (2015), p. 399-410
- Publication 2** G. Minelli, S. Krajnović, "Numerical Investigation of the Actuated Flow on a Bluff Body" in *The International Conference on Jets, Wakes and Separated Flows (ICJWSF2015)*, June 16-18, 2015, Stockholm, Sweden
- Publication 3** G. Minelli, S. Krajnović, B. Basara "Actuation of the flow field around a frontstep with a rounded leading edge" in *8th international symposium on Turbulence, Heat and Mass Transfer*, September 15-18, 2015, Sarajevo, Bosnia and Herzegovina



## ACKNOWLEDGEMENTS

I want to express my gratitude to my advisor, Prof. Siniša Krajnović, who gave me the opportunity to work on this project. Siniša, thank you for your constant support which formed my knowledge and my attitude in research. Thank you for every brilliant discussion which helped me to step further, and thank you for all the trust you put in me since we met the first time. I hope I will be able to live up to your expectations by my fervency in pursuing my Ph.D.

I am grateful to Linus Hjelm and Volvo Trucks for all the support and guidance received and for supporting the experimental part of the project. Thanks to Prof. Valery Chernoray and Ph.D student Erwin Adi Hartono for being so ready to transfer knowledge and experience in the lab. Many thanks go to Prof. Branislav Basara for solving any doubts regarding AVL Fire. Thanks also to the former Ph.D Eysteinn Helgason and Jan Östh for being so helpful during my first year. I am extremely thankful to all my colleagues at the Division of Fluid Dynamics, who create an inspiring work environment.

I am really grateful to my family, for being such great friends, advisers and supporters in all decisions I take.

Last but not least, I want to thank my fiancée Rita, "You light up my days".

This work is funded by the Swedish Energy Agency and supported by Volvo Trucks. Software licenses were provided by AVL List GMBH. Computations were performed at SNIC (Swedish National Infrastructure for Computing) at the Center for Scientific Computing at Chalmers (C3SE) and the National Supercomputer Center (NSC) at LiU.



*To my father, who shaped my soul without being here*



# Contents

Abstract	i
List of publications	iii
Acknowledgements	v
<b>I Extended Summary</b>	<b>1</b>
<b>1 Introduction</b>	<b>1</b>
1.1 Heavy truck: a bluff body . . . . .	2
1.2 Flow control . . . . .	3
1.3 Why actuation at the A-pillar? . . . . .	4
1.4 The flow topology . . . . .	5
1.5 Project outline . . . . .	6
<b>2 Turbulent flows: simulations and experiments</b>	<b>7</b>
2.1 Computational Fluid Dynamic: DNS, LES, PANS and RANS . . . . .	8
2.1.1 Large Eddy Simulation . . . . .	9
2.1.2 Bridging methods . . . . .	10
2.1.3 PANS $k - \varepsilon - \zeta - f$ . . . . .	12
2.1.4 Numerics . . . . .	14
2.2 Experiments . . . . .	14
<b>3 Modal decomposition</b>	<b>17</b>
<b>4 Summary of appended papers</b>	<b>19</b>
4.1 Paper A . . . . .	19
4.2 Paper B . . . . .	19
4.3 Paper C . . . . .	19
4.4 Paper D . . . . .	20
<b>5 Conclusions and Future work</b>	<b>21</b>
References	23



# Part I

## Extended Summary

### 1 Introduction

Transport is the cornerstone that defines our modern standard of life. Transport broadens the global market and our personal view of the world. Large distances become small, and most of our needs, desires and dreams are effortlessly covered. Transport is also the treadmill on which our modern economy runs, but to keep it running we need to join sustainability with mobility. The harmful aspects of a non sustainable development are widely acknowledged based on the experience of the latest 30 years. Thus, decreasing emissions became a strict requirement during the latest years. Nowadays, a large part of the research in transportation focuses on sustainability; the goal is to reduce emissions while still, increasing transportation. Europe is playing a leading role in this common goal, with the final objective to reduce emissions by 60% by 2050, which is ambitious yet possible. The actual emission situation in Europe highlights the Green House Gasses (GHG) emitted by road vehicles, Fig. 1. Transportation represents 1/4 of the total emissions, and the large majority (73%) is represented by road transportation. See the target line (dashed black line) in Fig. 1. The final goal is still far away; thus, improving the aerodynamic features of heavy trucks and road vehicles is a necessary contribution toward the target.

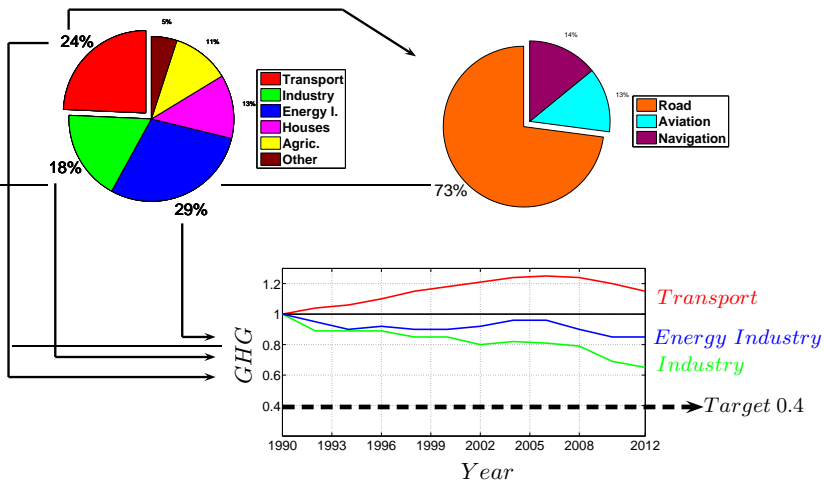


Figure 1: The GAG European situation. Trend from 1990 to 2012. Data collected from [1]

## 1.1 Heavy truck: a bluff body

From an aerodynamic point of view, bodies that move through a fluid (air in this case) are classified in two main categories: streamlined bodies (Fig. 2a) and bluff bodies, (Fig. 2b)

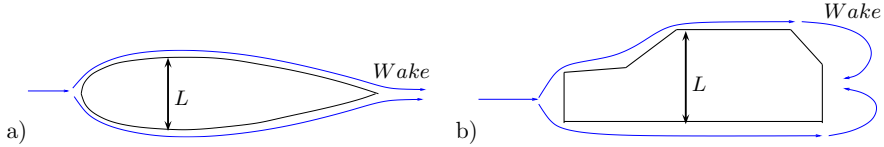


Figure 2: a) *streamlined body*. b) *bluff body*

At this point it is necessary to define *aerodynamic drag* and *wake*. Aerodynamic drag is the fluid drag force that acts on any moving solid body in the direction of the fluid freestream flow, [2]. The drag consists of two terms: the frictional and the pressure component. The wake is by definition the region of fluid behind a moving body, characterized by high velocity fluctuations arising from boundary layer flow separation. The main difference between the above categories therefore consists of the dimension of the wakes they produce and the dominant drag component they experience. A streamlined body, produces a thin wake which confers a low value of drag. The boundary layer does not separate from the surface of the body, and the main source of drag is the frictional component. On the other hand, when the body's wake is comparable to its characteristic dimension, it is generally called bluff body. All road vehicles and heavy trucks are classified as bluff bodies. They produce a large wake, with a large separation of the boundary layer. In this case the pressure component of the drag is dominant. The tractive resistance of a heavy truck is distributed on rolling resistance at 65% and on aerodynamic forces at 35%. Thus, a reduction of the aerodynamic losses by 20% allows a fuel consumption reduction by 6% [3]. Analyzing the main sources of resistance of motion, one can understand the large impact of the aerodynamic on power consumption. The main sources of drag in a heavy truck, principally arise from four different regions: the base region, wheel housing and under-body, the gap between the tractor and trailer and the front of the tractor, Fig 3.

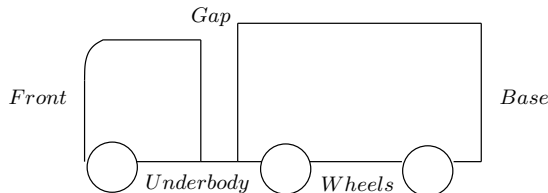


Figure 3: *The main source of aerodynamic drag in a heavy truck*

Aerodynamic research has investigated solutions to improve the aerodynamic performance of these regions. The main objective is to reduce drag, manipulating, or better controlling, the flow to a more desired state. Thus, flow control techniques are used and employed in several ways with advantages and drawbacks. A deeper description of flow control is given in the upcoming section.

## 1.2 Flow control

Many definitions have been used to describe flow control. Following the words of Gad-El-Hak [4], flow control is *the attempt to favorably alter the character or disposition of a flow field that is of concern*. One of the first human empirical attempts toward a favorable flow control can be found in the fin-stabilizer of arrows. Empirical attempts are brought slowly to science, and the science of flow control started in 1904, when the boundary layer theory and the scientific method to control a flow field were introduced by Prandtl [5]. The economic crisis and wars of the 20<sup>th</sup> century pushed forward every scientific field, faster than any other century before. The science of flow control was not an exception. During the years it broadened its applications and new methodologies were discovered to overcome challenges and to open new possibilities. The challenge of today is to extensively bring flow control to civil transport, from aeroplanes to passenger cars with no exception for commercial transport vehicles such as trains and heavy trucks. For trucks in particular, the challenge is amplified by the restriction of the design regulations. A truck is indeed designed for cargo and stocking operations, distancing its shape from being aerodynamic. Therefore, part of the challenge consists of keeping the cargo optimized shape, reducing the aerodynamic drag. Starting from the late 1970s with the advent of the oil crisis, and continuing during the 1980s, extensive research was performed on heavy vehicles [6–8]. This period has seen the evolution of several devices, add-ons and design alterations applied to trucks. For example, in the early 1980s, the front corner of the trailer was smoothed to a rounded shape. Flaps bridging the gap between the tractor and trailer are extensively used today. Flaps applied at the trailing edge [9], flow treatment devices for the under-body or the trailer base [10], cavities [11, 12], boat tails [13] and other add-ons [14] have recently been investigated in order to delay the flow separation, thus reducing the wake effect. However such techniques have tried to reduce the drag with varying success; they all have a common drawback: they are passive flow control techniques, thus designed to work at a nominal condition which seldom matches the real operating flow state. Here rises the importance of designing a control adaptable to the flow condition, an Active Flow Control (AFC). Indeed, the AFC opens the possibility for feedback control (open-loop) once the closed-loop flow mechanisms are well understood. The AFC can be classified in to three main categories: flow control by means of moving surfaces [15, 16], by means of plasma actuators (reviews are provided in [17–19]), and by means of synthetic jets. The main disadvantage of the former technique lies in its applicability due to geometrical constraints. The moving surfaces need mechanical transmission and electric engines which are not easy to embed in the original vehicle geometry. Plasma actuator research for flow control started 20 years ago [20] and produced promising results. This is however, far from being extensively applicable in the near future. For example, more research is needed to

understand the degradation of the actuation over time and their power consumption [21]. Thus, the synthetic jets turned out to be the most effective way to manipulate the flow field. The AFC used in this work is a Zero Net Mass Flux (ZNMF) synthetic jet. In comparison with the work of Krajnović et al. [22], the ZNMF does not employ steady suction or blowing but moves air by means of an oscillating membrane. Promising results of this technique were found in several studies, for both airfoils [23, 24], bluff bodies [25] and generic vehicles [26]. Their main achievement and potential future development are described in the reviews provided by Gad-el-Hak [4], by Cattafesta and Sheplak [27] and more recently by Brunton and Noack [28].

### 1.3 Why actuation at the A-pillar?

When a truck moves with a certain speed  $U_{inf}$ , the flow impinges the front of the tractor and migrates toward the A-pillars. At this point the flow separates, creating a recirculation flow region that increases the drag, Fig. 4. With rounded A-pillars, the aerodynamics of the front improves and the separation is controlled to some extent. Cooper [6] describes the use of rounded corners, showing the effectiveness of this acknowledged expedient. So the question that now emerges is: why do we still need to control the flow in this region?. The answer is twofold. Normally the flow impinging the front is not oriented along the direction of the truck (even when the vehicle is moving at cruise speed), due to side wind, gusts or steering. In this situation the truck experiences an angle with respect to the direction of the flow. This angle is generally called the yaw angle. The yaw angle measured during cruise speed varies between  $5^\circ$  and  $10^\circ$ , which is enough to induce the separation visualized in Fig. 4 and worsen the aerodynamic performance. The second aspect is that using an AFC, the radius of the A-pillar can be decreased, gaining space inside the truck’s cabin while having the required aerodynamic performance.

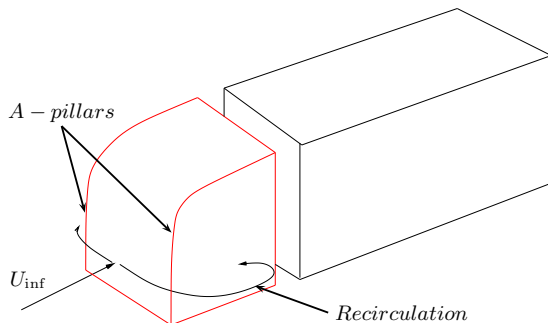


Figure 4: *The flow separation arising at the A-pillar*

If Fig. 4 shows the natural behavior of the flow field, Fig. 5 shows the effect of the actuation. The synthetic jet, placed before the natural separation point of the flow, introduces a disturbance (violet arrows in Fig. 5) by means of blown and sucked air. This vibration has a certain frequency and a certain magnitude, which interact with the flow.

Using a suitable value for both these two parameters, the control interacts effectively with the flow, delaying and eventually suppressing separation (blue dashed line in Fig. 5).

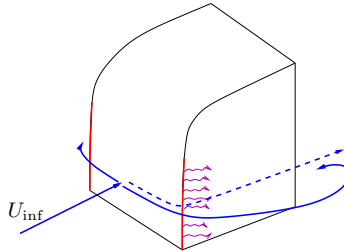


Figure 5: *The effect of the actuation*

## 1.4 The flow topology

Section 1.3 presented the general behavior of the studied flow case. Key features and important details of the flow can be extracted looking at the topology of the flow structures. The A-pillar separation can be connected, to some extent, to the flow behavior visualized in stalled airfoils by different authors [23, 29–31], Fig. 6a. The main features that characterize the topology of this flow are the separated shear layer, the near/side wake shedding and their interaction. Figure 6b depicts a top view of a generic truck cabin and a flow topology similar to the one described by stalled airfoils. The natural frequency of the shear layer is usually higher compared to the near wake shedding, but the coupling of them results in a collective interaction during the formation of the vortices, as was observed by Unal and Rockwell in [32].

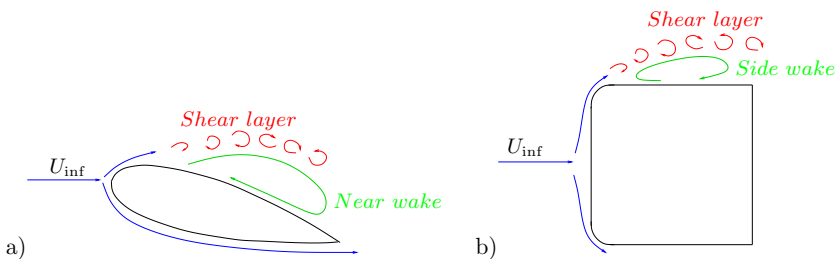


Figure 6: *The flow topology*

With a modal decomposition of the flow (Chapter 3), it is possible to separate and associate frequencies to structures. This tool is particularly useful for distinguishing the two main flow patterns described in Fig. 6. The structures present in the shear layer are smaller, containing a smaller amount of energy, yet are dynamically important for the near/side wake formation. Thus, when influencing the shear layer with AFC, the larger vortices of the near/side wake are also affected. In particular, the present study shows that actuating the flow using the shear layer frequency (Paper A and Paper D) gives a

higher reduction of the recirculation bubble and drag, while higher and lower actuation frequencies are not as effective.

## 1.5 Project outline

This thesis is part of a five-year Ph.D project where the overall objective is to reduce aerodynamic drag on heavy vehicles by the use of the so called Active Flow Control technique. AFC has been used extensively and successfully on airfoils, in order to enhance their performance, preventing flow separation. Therefore, the focus of this Ph.D project is to adapt a Zero Net Mass Flux synthetic jet on heavy vehicles. The investigation of its potential, the impact on the performance, and the real implementation at the A-pillar of a real truck are of main importance. Experiments were made in the Chalmers University closed loop wind tunnel and Computational Fluid Dynamics (CFD) unsteady simulations (LES and PANS) are conducted throughout the project.

## 2 Turbulent flows: simulations and experiments

It is very common to observe turbulent flows in our everyday surroundings: from waterfalls to the smoke rising from a chimney, from the motion of sea waves to the flow around moving vehicles, and other engineering applications. There is no exact definition of turbulence, but a turbulent flow has common and well defined characteristics as follows.

- A turbulent flow is three dimensional.
- A turbulent flow is unsteady and contains high spatial and temporal fluctuations. The fluid velocity field varies significantly and irregularly in both position and time.
- A turbulent flow has the ability to mix and transport fluid more than a comparable laminar flow [33].
- A turbulent flow is dissipative, meaning that it loses part of its energy (kinetic energy) to internal energy (heat), through the cascade process, Fig. 1.
- As a consequence of the latter, turbulence needs always to be sustained by additional kinetic energy.
- A turbulent flow is chaotic and unpredictable.

The difference between laminar and turbulent flows has been observed for centuries but only in 1894 did Reynolds define the characteristics of the transition between the two flow states [34]. He also realized and made experiments of the non dimensional parameter (Reynolds number  $Re$ ), that defines the transition based on the flow (using a velocity scale  $\mathcal{U}$ ), the fluid (using the kinematic viscosity  $\nu$ ) and the geometry (using a length scale  $\mathcal{L}$ ),

$$Re = \frac{\mathcal{U}\mathcal{L}}{\nu} \tag{1}$$

$Re$  also represents the ratio between inertial and viscous forces. Thus, high- $Re$  turbulent flows are mainly characterized by inertial forces while the viscous forces prevail in the low- $Re$  ones. As mentioned above, turbulence defines most engineering flows, with no exception for flows around vehicles and trucks. Thus, in vehicle aerodynamics,  $Re$  is of major importance in defining a flow field. In this case the free-stream velocity and the characteristic dimension of the vehicle (width or height) are taken as  $\mathcal{U}$  and  $\mathcal{L}$ , respectively.

A summary of the main Computational Fluid Dynamic (CFD) approaches to studying a turbulent flow and a description of the experimental techniques used throughout the project are given in the next sections.

## 2.1 Computational Fluid Dynamic: DNS, LES, PANS and RANS

CFD uses different approaches to resolve a turbulent flow field. In general, the choice of method is a compromise between the level of flow resolution and the computational resources available.

It is widely accepted that the equations system, known as Navier-Stokes Equations (NSE), mathematically determines the motion of fluids, although no mathematical proof exists for their universal validity. For an incompressible, single-phase flow with constant density  $\rho$  and viscosity  $\mu$ , the system reads:

$$\frac{\partial u_i}{\partial x_i} = 0 \quad (2)$$

$$\frac{\partial u_i}{\partial t} + u_j \frac{\partial u_i}{\partial x_j} = -\frac{1}{\rho} \frac{\partial p}{\partial x_i} + \nu \frac{\partial^2 u_i}{\partial x_j \partial x_j} + f_i. \quad (3)$$

Equation 2 is the continuity equation and expresses the mass conservation. Equation 3 is the momentum equation and expresses the momentum conservation.  $u_{i=x,y,z}$  are the three components of the velocity vector in a Cartesian coordinate system, and  $p$  denotes the hydrodynamic pressure.  $\nu = \mu/\rho$  is the kinematic viscosity of the fluid and  $f_i$  are possible body forces (e.g. gravitational force). The NSE mathematically represent the large variety of flow structures (flow scales  $\kappa$ ) observed in a turbulent flow. Figure 1 shows the so called energy cascade process and how the flow scales are defined by their energy level  $E(\kappa)$ . Three main regions describe the aforementioned process. The energy is introduced in the flow by the largest eddies in the energy-containing region (*I*) and is consequentially transferred from larger to smaller eddies (typically anisotropic) through the entire inertial subrange, (*II*). The energy is eventually dissipated into heat by the so called Kolmogorov scales (typically isotropic) in the dissipation range, (*III*).

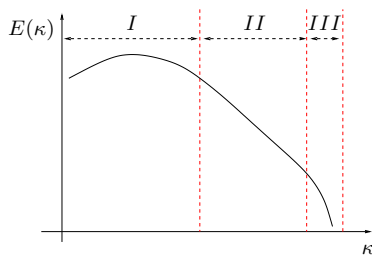


Figure 1: *The energy spectrum of a turbulent flow. Energy-containing region (I), inertial subrange(II) and dissipative range (III)*

The Direct Numerical Simulation (DNS) is used when the NSE are written in a discrete form and integrated numerically without modeling or hypothesis, [35]. DNS is the most accurate approach, although it requires a prohibitive amount of computational resources to resolve all the scales present in the flow, from the largest to the Kolmogorov scales.

As an example, a truck moving at cruise speed ( $Re = 3 \times 10^6$ ) produces a turbulent flow containing large structures of the dimension  $10^0 m$  and small structures of the dimension  $10^{-9} m$ . Such a variety of scales makes DNS infeasible for complex or high- $Re$  flows. Therefore, DNS is only used to study fundamental flows such as isotropic turbulence [36], turbulent boundary layer [37, 38] and pipe flow [39]. Nevertheless, different simplifications exist to enable solving Eqs. 2 and 3 in an affordable manner. One of this is the so called Reynolds decomposition, which splits up the flow in a mean and a fluctuating part as:

$$u_i = \bar{u}_i + u'. \quad (4)$$

Inserting Eq. 4 into the NSE gives the Reynolds Averaged Navier-Stokes (RANS) equations

$$\frac{\partial \bar{u}_i}{\partial x_i} = 0 \quad (5)$$

$$\frac{\partial \bar{u}_i}{\partial t} + \bar{u}_j \frac{\partial \bar{u}_i}{\partial x_j} = -\frac{1}{\rho} \frac{\partial \bar{p}}{\partial x_i} + \frac{\partial}{\partial x_j} \left( \nu \frac{\partial \bar{u}_i}{\partial x_j} + \frac{1}{\rho} \tau_{ij} \right). \quad (6)$$

The additional term, the so called Reynolds stress tensor, is obtained:

$$\tau_{ij} = -\rho \left( \overline{u'_i u'_j} \right). \quad (7)$$

The six new unknowns introduced by tensor  $\tau_{ij}$  make the system impossible to solve. Hence, the Reynolds stresses need to be modeled to close the problem. For this purpose the Boussinesq assumption [40] is often used to model the turbulent diffusion with a newly introduced eddy viscosity. This approach is widely used for applications of industrial importance. RANS approach resolves only the mean value of the flow, the large scales ( $I$  in Fig. 1), modeling the entire cascade process and the dissipation. In this manner the efficiency of the calculation increases to the detriment of the accuracy. Moreover, RANS provides a solution for the mean flow, and turbulence is treated in a stochastic sense only. Even though this is acceptable in many industrial applications, RANS cannot be used for a wide range of fields. Examples of such fields are active flow control [41], aeroacoustic [42], and fluid structures interaction studies [43].

If DNS and RANS are the antipodes of the simulation techniques, Partially Averaged Navier-Stokes (PANS) and Large Eddy Simulations (LES) represent good compromises between computer resources and accuracy. The central assumption in these methods is the scale's distinction in large and small scales. As mentioned above, the large scale motions carry most of the energy and the anisotropy of the flow, while the small scales represent the isotropic part of the turbulence and are responsible for the dissipation process. Hence, modeling the small scales and resolving the large ones can benefit the overall result of the simulation, reducing the simulation time as compared to DNS and improving the accuracy as compared to RANS.

### 2.1.1 Large Eddy Simulation

To achieve the small/large scale separation, LES requires a filtering operation. As for the Reynolds decomposition, the LES filtering reformulates the expression of the instantaneous flow field,

$$u_i = \bar{u}_i + u'' \quad (8)$$

where the velocity field is decomposed in a resolvable part  $\bar{u}_i$  and an unresolved, or so called Sub Grid Scale (SGS), fluctuating part  $u''$ . From now, the bar notation denotes a filtering operation and not averaging in time, as for the Reynolds decomposition. Applying the filtering to Eqs. 2 and 3, the filtered incompressible NSE read:

$$\frac{\partial \bar{u}_i}{\partial x_i} = 0 \quad (9)$$

$$\frac{\partial \bar{u}_i}{\partial t} + \bar{u}_j \frac{\partial \bar{u}_i}{\partial x_j} = -\frac{1}{\rho} \frac{\partial \bar{p}}{\partial x_i} + \frac{\partial}{\partial x_j} \left( \nu \frac{\partial \bar{u}_i}{\partial x_j} + \frac{1}{\rho} \tau_{ij} \right). \quad (10)$$

This set of equations is different from the previous RANS because of the different meaning of the overbars and the additional term  $\tau_{ij}$  that represents the SGS stress tensor:

$$\tau_{ij} = -\rho (\overline{u_i u_j} - \bar{u}_i \bar{u}_j). \quad (11)$$

Using the eddy viscosity models as for the standard Smagorinsky model [44],  $\tau_{ij}$  can be modeled as

$$\tau_{ij} - \frac{1}{3} \tau_{kk} \delta_{ij} = -\nu_t \left( \frac{\partial \bar{u}_i}{\partial x_j} + \frac{\partial \bar{u}_j}{\partial x_i} \right) = -2\nu_t \bar{S}_{ij}, \quad (12)$$

where  $\bar{S}_{ij}$  is the strain stress tensor, and the eddy, or turbulent, viscosity  $\nu_t$  is modelled as

$$\nu_{sgs} = l^2 \bar{S} = (C_s f \Delta)^2 |\bar{S}|. \quad (13)$$

Here the length scale constant,  $l$ , is taken to be the product of the the Smagorinsky constant,  $C_s = 0.1$ , previously used in bluff body LES [43, 45, 46], the local grid size  $\Delta = (\Delta_x \Delta_y \Delta_z)^{1/3}$  and the Van Driest damping function

$$f = 1 - \exp\left(\frac{-n^+}{25}\right), \quad (14)$$

where  $n^+$  is the wall normal distance in viscous units.

The grid point requirement for a good resolved LES scales with  $Re^{13/7}$  as proposed by Choi and Moin [47], while Piomelli and Balaras [48] found the grid point estimation for a DNS scaling with  $Re^{9/4}$ . The LES estimation slightly relaxes the computational efforts as compared to DNS, yet it does not drastically decrease the cost. In fact, Spalart et al. [49] estimate LES to be infeasible for an entire aircraft wing until the year 2045, and, they continue to say that *"terminating efforts in RANS turbulence modelling would be a very misguided step"*. For this reason, research in modeling must continue and the new frontier of the latest years is hybrid models that carefully blend DNS/LES and RANS approaches. An example is the Partially Averaged Navier Stokes (PANS) approach, illustrated in the upcoming section.

## 2.1.2 Bridging methods

Bridging the gap between academic research and industrial R&D is of major importance. The main challenge is to provide and develop a suitable and "intelligent" tool for industrial

flow simulation, that, independently switches its approach from DNS to RANS, or better said Unsteady RANS (U-RANS), based on the available mesh resolution. The two main currents of bridging methods are the Detached Eddy Simulation (DES) and the PANS approach developed and modified in all their flavors over the years. The first attempt to develop DES was introduced by Spalart et al. [49]. The basic idea is for the model to act as a U-RANS in boundary layers and LES-like, otherwise. In principle, the LES or RANS choice is based on a comparison between the wall distance and the grid spacing. The main drawback of this behavior is that DES grids need to be carefully designed, knowing a priori where the flow separates (LES should resolve the large separated vortices) and in which areas it remains attached (RANS boundary layer resolution). Many variations of this approach have been offered during the years and a review of variations and flavors is provided in [50]. Although zonal-like approaches have attracted great interest from many authors and developers with remarkable results [51–53], they are still limited concerning adaptivity to the mesh. In other words, the mesh should always be designed carefully. In order to overcome these difficulties and to make the solver act "independently" the PANS approach was developed. The foundation of this method relies on the U-RANS approach. The goal of U-RANS is to resolve smaller scales that are normally averaged by a steady RANS simulation. While the idea behind the method is promising, U-RANS showed inaccurate predictions of severely separated flows. The main reason for this is that U-RANS lies on the evolution of the eddy-viscosity, which evolves in large values, much larger than the actual mesh resolution could have supported. In this way, most of the temporal and spatial fluctuations are suppressed, altering the final solution. In an effort to resolve most of the fluctuating scales, the RANS coefficients have to be modified according to the resolution of the grid, in a physically correct manner [54]. Modifying the parameters of the parent RANS model, PANS introduces a dynamic approach that prevents an uncontrolled growth (RANS like result) or drop (spurious fluctuation) of the eddy viscosity, based on the spatial resolution of a given grid and the physics of the flow.

The smart idea to develop a hybrid method as such started with Girimaji [55] with the first PANS model based on the  $k - \varepsilon$  RANS equations. The  $k - \varepsilon$  PANS method has been successfully tested on different standard bluff body flows, such as flow around a square cylinder [56] and a circular cylinder [57]. Theoretical proof and a physical explanation of his improvement in comparison with RANS are given in [54]. Still, the quality of PANS also depends on its RANS parent model. As a consequence, several flavors of the PANS method have been developed:

- Lakshmipathy and Girimaji [58] introduced the  $k - \omega$  PANS method. The results of this were compared with U-RANS showing that  $k - \omega$  PANS is able to resolve more vortical structures, enhancing the experiments agreement.
- Ma et al. [59] employed a low Reynolds number  $k - \varepsilon$  model to correct the standard  $k - \varepsilon$  PANS wall behavior.
- Durbin [60] proposed a  $k - \varepsilon - \bar{v}^2 - f$  PANS, that was later reformulated by Hanjalic [61], to enhance the wall behavior and to take into account the Reynolds number effect in the viscous and buffer sub-layers.
- Basara et al. [62] proposed the  $k - \varepsilon - \zeta - f$  PANS developed on the namesake

RANS model. The model has been validated for simple cases (channel flow) and more complicated cases (flow around a finite cylinder) [63].

The latter variation is also employed in this thesis. Thus, a more detailed description is given in the following section.

### 2.1.3 PANS $k - \varepsilon - \zeta - f$

Thanks to promising results, the PANS  $k - \varepsilon - \zeta - f$  method has gained much attention in bluff body flow simulations. The results reported in [64–66] show the superiority (best compromise between accuracy and resources) of the bridging method when compared to RANS and LES. However, the method is still under development and some challenging cases are listed in [67]. The model is also employed for the simulations on which Papers B-C-D are based.

Before expressing the equations which define the model, it is necessary to recall the Germano’s averaging invariance property [68]. He stated that the SubFiltered Scale (SFS) term must be invariant to the type of filtering. Thus, if the filtering applied to the NSE is commutative with the spatio-temporal differential operator, and decomposing the turbulent velocity field  $V_i$ , by an arbitrary filter, in a resolved  $U_i$  and unresolved field  $u_i$ ,

$$V_i = U_i + u_i \quad (15)$$

the NSE evolves according to [68] into the so called PANS equation [69]:

$$\frac{\partial U_i}{\partial t} + U_j \frac{\partial U_i}{\partial x_j} = -\frac{1}{\rho} \frac{\partial p}{\partial x_i} + \frac{\partial}{\partial x_j} \left( \nu \frac{\partial U_i}{\partial x_j} + \tau(V_i, V_j) \right), \quad (16)$$

where  $\tau(V_i, V_j)$  is the generalized second moment [68] and represents the effect of the unresolved scales on the resolved field. As it was for LES, Eq. 12, the Bousinnesq assumption is now invoked to model the second moment:

$$\tau(V_i, V_j) = -2\nu_u S_{ij} + \frac{2}{3} k_u \delta_{ij}. \quad (17)$$

Here  $k_u$  is the unresolved kinetic energy,  $S_{ij}$  is the resolved stress tensor,

$$S_{ij} = \frac{1}{2} \left( \frac{\partial U_i}{\partial x_j} + \frac{\partial U_j}{\partial x_i} \right), \quad (18)$$

and  $\nu_u = C_\mu \zeta_u \frac{k_u}{\varepsilon_u}$  is the viscosity of the unresolved scales where  $\zeta = \overline{v_u^2}/k_u$  is the velocity scale ratio of the unresolved velocity scale  $\overline{v_u^2}$  and  $k_u$ .  $\overline{v_u^2}$  refers to the normal fluctuating component of the velocity field to any no-slip boundary. At this stage, three transport equations for  $k_u - \varepsilon_u - \zeta_u$  and a Poisson equation for the elliptic relaxation function of the unresolved velocity scales are necessary to close the model. Thus the complete PANS

$k - \varepsilon - \zeta - f$  model is given by the following set of equations:

$$\begin{aligned}
\nu_u &= C_\mu \zeta_u \frac{k_u^2}{\varepsilon_u} \\
\frac{\partial k_u}{\partial t} + U_j \partial k_u \partial x_j &= P_u - \varepsilon_u + \frac{\partial}{\partial x_j} \left( \frac{\nu_u}{\sigma_{k_u}} \frac{\partial k_u}{\partial x_j} \right) \\
\frac{\partial \varepsilon_u}{\partial t} + U_j \partial \varepsilon_u \partial x_j &= C_{\varepsilon 1} P_u \frac{\varepsilon_u}{k_u} - C_{\varepsilon 2}^* \frac{\varepsilon_u^2}{k_u} + \frac{\partial}{\partial x_j} \left( \frac{\nu_u}{\sigma_{\varepsilon_u}} \frac{\partial \varepsilon_u}{\partial x_j} \right) \\
C_{\varepsilon 2}^* &= C_{\varepsilon 1} + f_k (C_{\varepsilon 2} - C_{\varepsilon 1}); \quad C_{\varepsilon 1} = 1.4 \left( 1 + \frac{0.045}{\sqrt{\zeta_u}} \right) \\
\frac{\partial \zeta_u}{\partial t} + U_j \partial \zeta_u \partial x_j &= f_u - P_u \frac{\zeta_u}{k_u} + \frac{\zeta_u}{k_u} \varepsilon_u (1 - f_k) + \frac{\partial}{\partial x_j} \left( \frac{\nu_u}{\sigma_{\zeta_u}} \frac{\partial \zeta_u}{\partial x_j} \right) \\
L_u^2 \nabla^2 f_u - f_u &= \frac{1}{T_u} \left( c_1 + c_2 \frac{P_u}{\varepsilon_u} \right) \left( \zeta_u - \frac{2}{3} \right).
\end{aligned} \tag{19}$$

$P_u = -\tau(V_i, V_j) \frac{\partial U_i}{\partial x_j}$  is the production of the unresolved turbulent kinetic energy and it is closed by the Boussinesq assumption, Eq. 17.  $\sigma_{k_u, \varepsilon_u} = \sigma_{k, \varepsilon} \frac{f_k^2}{f_\varepsilon}$  are the counterpart of the unresolved kinetic energy and dissipation, respectively. In this way  $f_{k, \varepsilon}$  contributes to changing the turbulent transport Prandtl number contributing to the decrease of the unresolved eddy viscosity [59]. The constants appearing in Eqs. 19 are:

$$C_\mu = 0.22; \quad C_{\varepsilon 2} = 1.9; \quad c_1 = 0.4; \quad c_2 = 0.65; \quad \sigma_k = 1; \quad \sigma_\varepsilon = 1.3; \quad \sigma_{\zeta_u} = 1.2.$$

$L_u$  and  $T_u$  are the length and time scales defined by using the unresolved kinetic energy:

$$L_u = \max \left[ \frac{k_u}{\varepsilon}, C_\tau \left( \frac{\nu}{\varepsilon} \right)^{1/2} \right]; \quad T_u = C_L \max \left[ \frac{k_u^{3/2}}{\varepsilon}, C_\eta \left( \frac{\nu^3}{\varepsilon} \right)^{1/4} \right],$$

where

$$C_\tau = 6; \quad C_L = 0.36; \quad C_\eta = 85.$$

A deeper explanation of the construction of the equations is given in [62, 63]. The parameters  $f_{k, \varepsilon}$  are the key factors that make the model act dynamically.  $f_{k, \varepsilon}$  are the ratios between resolved to total kinetic energy and dissipation, respectively, and they can assume values between 1 and 0 according to the selected cut-off. These parameters can be chosen a priori, knowing the resolution of the given grid. Yet, it might be more efficient to have a solver that adapts its accuracy to the flow case and the given grid, that has as a worse output of a RANS simulation. Here comes the importance of having a dynamic parameter which carries the characteristics of both the flow and the grid, adapting to the resolvable level of structures. For a further but justified simplification  $f_\varepsilon$  is assumed to be constant and equal to 1. Recalling that the spatial resolution to resolve the dissipative scales and the inertial subrange is a near-wall DNS resolution, these scales are unlikely to be resolved in most cases. Thus, all the unresolved dissipation is chosen to be RANS dissipation and therefore is modeled. Thus, the crucial step in developing an efficient model is the design of the last parameter,  $f_k$ . At every time-step for every

computational cell, the simulation evaluates the smallest value of  $f_k$  that the grid can support. The dynamic parameter was soon proposed as the ratio between the geometric averaged grid cell dimension,  $\Delta = (\Delta_x \Delta_y \Delta_z)^{1/3}$ , and the Taylor scale of turbulence,  $\Lambda = \frac{(k_u + k_{res})^{3/2}}{\varepsilon}$  [70]:

$$f_k(x, t) = \frac{1}{\sqrt{C_\mu}} \left( \frac{\Delta}{\Lambda} \right)^{2/3}. \quad (20)$$

### 2.1.4 Numerics

All types of numerical simulations require discretization of the spatial and temporal domain. Thus the choice of the suitable numerical scheme for every calculation is of primary importance. In this work, the CFD simulations are carried out using the commercial finite-volume software AVL-Fire. The NSE are discretized by the solver using a collocated grid arrangement. In the case of LES, the convective term present in Eq. 10 is discretized using Central Difference Scheme (CDS) with a blending factor of 0.96, meaning that 4% of first-order upwinding scheme is used to dampen the numerical oscillations and to overcome the local insufficient grid resolution. In the case of PANS, a second-order upwinding scheme is used for both the convective terms of the momentum equation and the turbulence closure system equations. For all simulations, the time discretization is done using the implicit second-order accurate three-time level scheme:

$$\left( \frac{d\phi}{dt} \right)_n = \frac{3\phi^n - 4\phi^{n-1} + \phi^{n-2}}{2\Delta t_n}; \quad \Delta t_n = t - t_{n-1} = t_{n-1} - t_{n-2}. \quad (21)$$

## 2.2 Experiments

Experiments are carried out in the Chalmers University closed circuit wind tunnel with test section dimensions of  $3.00 \times 1.80 \times 1.25 \text{ m}^3$  and a speed range of 0-60 m/s, see Fig. 2. The oncoming flow turbulence level was within 0.5%.

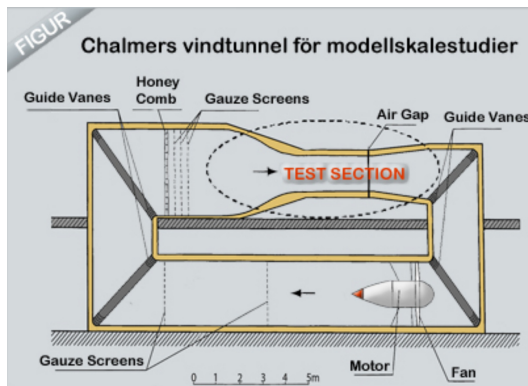


Figure 2: *Chalmers wind tunnel and its test section*

The actuator used in the experiments is a synthetic jet actuator based on a loud speaker enclosed in a cavity. Figure 3a) shows a CAD representation of the model placed in the Chalmers wind tunnel test section. A top view of the model is shown in Fig. 3b). The latter shows how the loudspeakers are placed inside the test box, the movement of their membranes recreates a blown and sucked air cycle at the slot located at the front rounded corner.

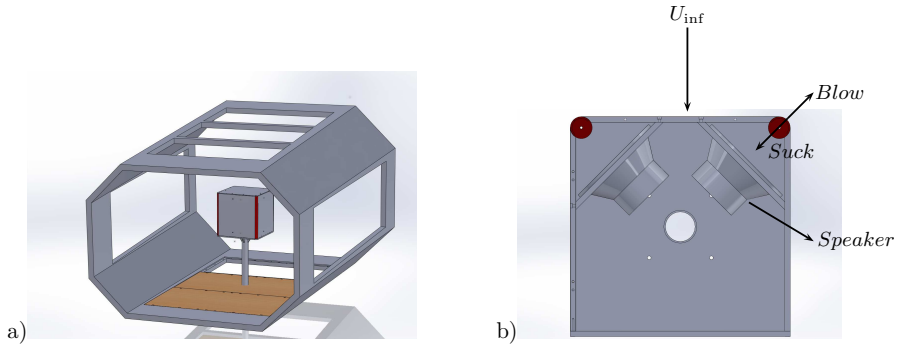


Figure 3: *The experimental model. a) overview of both model and wind tunnel test section. b) a top view of a cut plane on the model*

During experiments, the velocity of the actuation signal is measured at the actuator slot by traversing a hot-wire probe. The pressure on the body surface is monitored by a number of pressure taps as shown in Fig. 4.

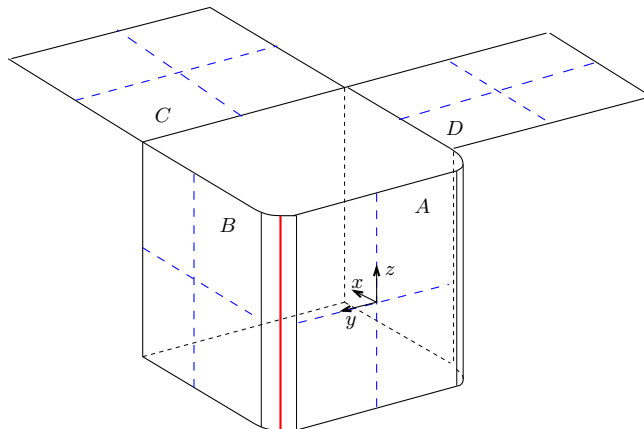


Figure 4: *The model of the truck cabin. Dashed blue lines represent pressure taps distribution. The solid red line represents the position of the actuation slot. A front side, B windward side, C base side, D leeward side*

The blue dashed lines in Fig. 4 represent a vertical and a horizontal pressure profile

for each named face. The model was first assembled and then placed in the Chalmers wind tunnel, as shown in Fig. 5

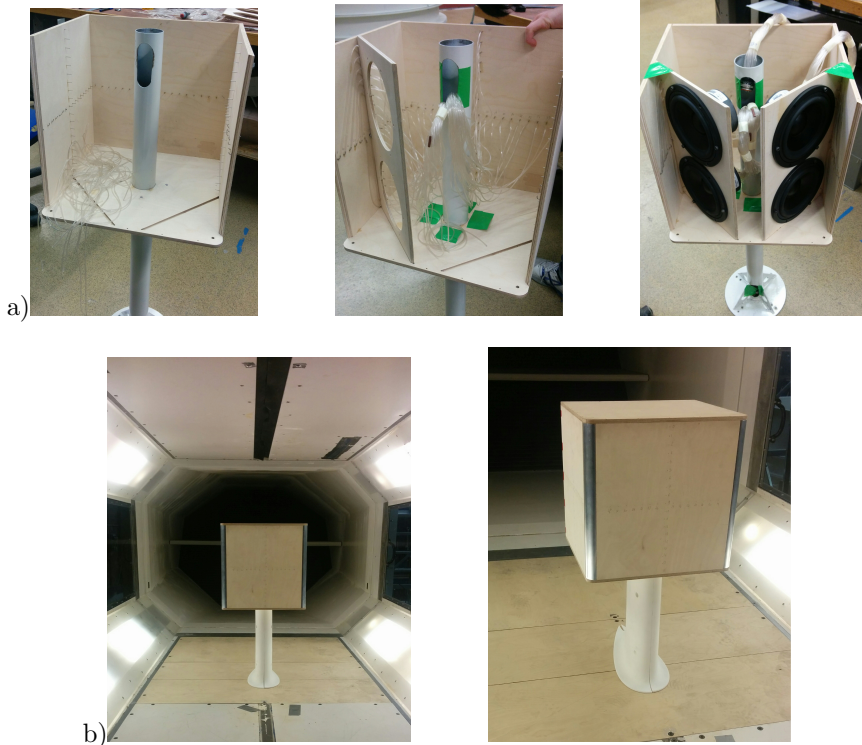


Figure 5: *a) Stages of the assembly process. b) The model placed in the wind tunnel*

An NACA 0024 is also used to cover the shaft and avoid undesired vortex shedding fluctuation. The flow Reynolds number is  $Re = 5 \times 10^5$  based on the free stream velocity and the width of the cabin,  $W = 0.4m$ , in the main series of experiments. At the current stage, the results are only compared for the unactuated flow configurations. Two different configurations at two different yaw angles,  $\beta = 10^\circ$  and  $\beta = 0^\circ$ , are tested. The measured pressure profiles are compared with PANS simulations. The results are discussed in detail in Paper D.

### 3 Modal decomposition

There are two main approaches to post-processing turbulence and turbulent flow data. The first is the stochastic approach, which ignores the fluctuating part of the flow, Eq. 7, extracting only statistically relevant informations. The second is the phenomenological approach, which analyzes and interprets the interaction of coherent and incoherent flow structures highlighting possible universal or case-specific turbulent patterns. In the framework of this project, the second approach is essential for two main reasons. The first motive is that a statistical approach is insufficient for studying the effect of a time varying actuation (AFC) on a turbulent flow. The second reason is that the knowledge of the structure's interaction sets the guidelines for a careful optimization process. The phenomenological approach gives hints and directions as to which are the main important structures acting in the flow, from both an energetic and a dynamic prospective. Modal and frequency decompositions are helpful tools in interpreting the flow mechanisms, that, for example, characterize a pressure gradient induced separation. One of the patterns pursued in this work is therefore to employ Proper Orthogonal Decomposition (POD) and Fast Fourier Transform (FFT) analysis to post-process CFD data.

The POD was developed independently for different disciplines (random variables, image processing, signal analysis chemical engineering and oceanography) by different authors. Among the first was Kosambi [71], but Lumley was the first to introduce POD in the context of turbulence [72]. An inspiring review of theory and applications of this method is presented in [73]. The approach used in this work, and increasingly commonplace in fluid dynamic research, is the snapshot methodology. In the latter, an ensemble of snapshots of a selected flow field region is gathered and consequentially processed. The snapshot method is not only suitable for CFD data, but is also largely employed in experiments, where the snapshots are collected by means of a high speed camera during a Particle Image Velocimetry (PIV) process, [74, 75]. Concerning CFD, several examples of successful POD applications are reported in the literature; modal decomposition has been applied to DNS data [76], LES and Hybrid methods (DES) [77]. In particular, LES were successfully post-processed by means of POD by Östh et al. [78, 79].

The result of a POD is not always straight-forward and is often complicated in terms of recognizing the dominant frequencies of every mode. Thus, in this work, POD is coupled with FFT analysis on the same set of snapshots. FFT is a robust method which, once applied to snapshots, is able to spatially identify the main frequencies characterizing a flow. The result of this analysis confirms and completes the information extracted by means of POD. Thus, POD and FFT analysis are used to produce a spatial, energy and dynamic map of the main flow structures.

The present POD is made of equidistantly sampled pressure snapshots  $p^m = p(\mathbf{x}, t^m)$  at time  $t^m = m\Delta t$ ,  $m = 1, \dots, M$ , with the time  $\Delta t$ , and a Cartesian coordinate system  $\mathbf{x} = (x, y, z)$  with unit vectors  $\mathbf{e}_x, \mathbf{e}_y, \mathbf{e}_z$ , respectively. As originally proposed by Lumley [80], this method is based on energy ranking of orthogonal structures computed from a correlation matrix of the snapshots. A Singular Value Decomposition (SVD) approach is used to conduct the POD analysis on the mentioned set of snapshots. In the present

POD, the pressure is decomposed into the mean field,  $\langle p \rangle$ , and the fluctuating part,  $p'$ , as

$$p(\mathbf{x}, t) = \langle p \rangle(\mathbf{x}) + p'(\mathbf{x}, t). \quad (1)$$

The fluctuating part is then approximated, by the SVD approach, with space dependent modes,  $p_i$ , and a time dependent mode coefficient,  $b_i$ , as

$$p'(\mathbf{x}, t) = \sum_{i=1}^{\infty} b_i(t) p_i(\mathbf{x}) \approx \sum_{i=1}^{N-1} b_i(t) p_i(\mathbf{x}) + p_{res}(\mathbf{x}, t). \quad (2)$$

The definition can now be written in a more compact form if we consider that  $b_0 = 1$  and  $p_0 = \langle p \rangle$  following [81],

$$p(\mathbf{x}, t) = \sum_{i=0}^{N-1} b_i(t) p_i(\mathbf{x}). \quad (3)$$

The first and second moments of the POD modes coefficients are:

$$\langle b_i \rangle = 0; \quad \langle b_i b_j \rangle = \mu_i \delta_{ij}. \quad (4)$$

The energy content of the single mode,  $K_i$ , is approximated from the mode coefficients as

$$K_i(t) = \frac{1}{2} b_i^2(t), \quad (5)$$

and the total energy,  $K_{\Sigma}(t)$ , is evaluated as

$$K_{\Sigma}(t) = \sum_{i=1}^{N-1} K_i(t). \quad (6)$$

## 4 Summary of appended papers

### 4.1 Paper A

*"Numerical investigation of active flow control around a generic truck A-pillar"*

The focus of this paper is the study of the A-pillar flow separation and its suppression, by means of an Active Flow Control (AFC), of a heavy transport vehicle. LES have been employed to study the physics of the separated flow. The model consists of a half section of a simplified truck, meeting the necessity of minimizing the computational cost without altering the flow physics. The LES were made at the Reynolds number of  $Re = 1 \times 10^5$  based on the width of the truck and the free stream velocity. The study of such a low  $Re$  is necessary to carry out a preliminary study that exposes the flow physics and minimizes the computational costs. The effect of the synthetic jet, zero net mass flux AFC has been studied using varying different parameters. the position of the slot and frequency of the actuation signal vary during the study in order to find the configuration that gives the highest reduction of drag. Modal decomposition is also successfully employed to study the interaction between different structures in the flow domain. An interpretation of the flow topology and its variation with the actuation frequency is also provided. The study shows that two main eddy patterns are responsible for the flow separation. An effective and optimal interaction, controlled by the actuation, was found to minimize the aerodynamic drag and the induced oscillations.

### 4.2 Paper B

*"Partially-Averaged Navier-Stokes Simulations of two bluff body flows"*

This paper examines the potential of the hybrid Partially Averaged Navier Stokes (PANS) methodology when applied to bluff body flows and vehicle aerodynamics. The PANS  $k - \varepsilon - \zeta - f$  model (section 2.1.3) has been employed. The paper discusses two flow configurations and underlines the possibilities of PANS when compared to LES and URANS. The separated flow around a sharp edge bluff body is well predicted by PANS, also when the grid resolution is poorer. The comparison with LES performed on the same grid clearly shows the promising potential of PANS, which is still under development. Interesting results concerning vehicle aerodynamics are also achieved. The study of the flow around a Willy's body shows the accuracy of PANS for Reynolds numbers that would require a much higher resolution when LES is employed. The ability of the method to adjust to the given computational grid allows an engineering approach to the simulation.

### 4.3 Paper C

*"Partially-Averaged Navier-Stokes Simulations of Flows Around Generic Vehicle at Yaw"*

The focus of this paper is to investigate the potential and limits of Partially Averaged Navier Stokes (PANS) when applied to a simplified vehicle at yaw. A Willy's body has been used for the computational study. Flow separation at the abrupt end of a surface, sharp edge separation, and adverse pressure gradient-induced separation are all flow mechanisms defining the separation of bluff bodies. The peculiarity of the Willy's body at yaw is to contain both pressure-induced separation and separation at the abrupt end of the rear. Thus, the study wants to investigate the PANS prediction of different separated flows when compared to Large Eddy Simulations (LES). Accurate results are shown for the trailing vortices and pressure-induced separated flow. The prediction of the second kind of separation at the abrupt end was found to be problematic. An interpretation of what causes the wrong prediction in the code is also provided for further developments.

## 4.4 Paper D

*"Experimental and Numerical Investigation of Active Flow Control on a Generic Truck Cabin"*

This work presents the achievement on drag reduction by means of Active Flow Control (AFC) on a generic bluff body. The model consists of a simplified truck cabin, characterized by sharp edge separation on top and bottom edges and pressure-induced separation on the rounded vertical front corner. The pressure-induced separation reproduces the flow separation occurring at the front A-pillar of a real truck. Hybrid Partially Averaged Navier-Stokes (PANS) simulations are compared with wind tunnel experiments. The Reynolds number for both simulations and experiments is  $Re = 5 \times 10^5$  based on the inlet velocity  $U_\infty$  and the width of the model  $W = 0.4m$ . A validation of the hybrid CFD model on two flow configurations is followed by a CFD study of the optimal actuation frequency able to minimize the aerodynamic drag. PANS accurately predicts the flow field measured in experiments, and a notable drag reduction by means of AFC is observed in the numerical study.

## 5 Conclusions and Future work

The overall objective of the present ongoing work is to investigate and prove the effectiveness and the actual feasibility of a synthetic jet Active Flow Control (AFC) technique when applied to the A-pillar of a travelling truck. The first part of the work, reported in this thesis, was fundamental to gaining a better understanding of the flow field and the potential of the actuation, as well as a deeper knowledge of PANS. The intermediate goals achieved in the first part are listed below.

- The physics describing the separation mechanism has been studied. (Paper A and Paper D).
- Taking advantage of the knowledge of the physics of the separation mechanism, an optimal configuration of a ZNMF AFC was found for a low (Paper A) and a higher (Paper D) Reynolds number case.
- A modal decomposition process that couples POD and FFT was proven to be proper for studying the coherent and incoherent structures present in the flow. (Paper A and Paper D).
- The PANS method was tested for different bluff body flow cases with promising results. (Paper B and Paper C).
- A first preliminary experimental study was conducted to validate CFD, with a particular interest in gaining knowledge about PANS when applied to the present case. Two yaw configurations have been considered. Preliminary results of two unactuated flow conditions show good agreement between experiments and PANS. (Paper D).
- A numerical study has been conducted on AFC when applied to a 3-D bluff body flow. An optimal actuation is also investigated. (Paper D).

Although many intermediate stages have been accomplished, much research must still be done. The main guidelines for the development of the project and the future challenges to be overcome are listed below.

- The next step is to verify the effectiveness of AFC when applied to the experimental model. As a consequence, the results obtained will be compared with PANS simulations.
- The validation and comparison of the PANS method with LES and experiments should involve different test configurations. Unactuated and actuated cases at yaw angles have also to be tested and compared.
- The effectiveness of the AFC has to be investigated when a yaw angle is applied to the model.

- A dynamic study of the flow can also be done and compared against several steady configurations. Of particular interest is to verify the response of the AFC to the dynamic change of the yaw angle. This investigation is interesting for the introduction of a closed loop control.
- A closed loop can be developed in order to make the AFC sensitive and adaptable to different flow configurations.
- Once PANS is validated, it can be employed extensively for the computational study of a real truck geometry.

# References

- [1] N. Hill, M. Morris, and I. Skinner, "SULTAN : Development of an Illustrative Scenarios Tool for Assessing Potential Impacts of Measures on EU Transport GHG," no. June, 2010.
- [2] J. D. Anderson, *Introduction to Flight*. 2005.
- [3] I. Hucho, "Aerodynamics of Road Vehicles," *Annual Review of Fluid Mechanics*, vol. 25, no. 1, pp. 485–537, 1993.
- [4] M. Gad-el Hak, "Introduction to flow control," *Flow Control*, no. 1904, pp. 1–107, 1998.
- [5] L. Prandtl, "ber Flüssigkeitsbewegung bei sehr kleiner Reibung," *Verhandlungen des dritten internationalen MathematikerKongresses*, vol. Heidelberg, pp. 484–491, 1904.
- [6] K. Cooper, "The effect of front-edge rounding and rear-edge shaping on the aerodynamic drag of bluff vehicles in ground proximity," 1985.
- [7] K. Cooper, "Truck Aerodynamics Reborn - Lessons from the Past," *SAE Technical Paper Series*, no. 724, 2003.
- [8] E. van der Spoel, M. P. Rozing, J. J. Houwing-Duistermaat, P. Eline Slagboom, M. Beekman, A. J. M. de Craen, R. G. J. Westendorp, and D. van Heemst, "Association analysis of insulin-like growth factor-1 axis parameters with survival and functional status in nonagenarians of the Leiden Longevity Study," *Aging*, vol. 7, no. 11, pp. 956–963, 2015.
- [9] M. El-alti, V. Chernoray, M. Jahanmiri, and L. Davidson, "Experimental and Computational Studies of Active Flow Control on a Model Truck-trailer," *EPJ Web of Conferences 25*, vol. 010, 2012.
- [10] R. Wood and S. Bauer, "Simple and low-cost aerodynamic drag reduction devices for tractor-trailer trucks," *SAE transactions*, vol. 112, no. 2, pp. 143–160, 2003.
- [11] B. Khalighi, S. Zhang, C. Koromilas, S. R. Balkanyi, L. P. Bernal, G. Iaccarino, and P. Moin, "Experimental and Computational Study of Unsteady Wake Flow Behind a Bluff Body with a Drag Reduction Device," *Society of automotive engineers*, no. 724, pp. 1–15, 2001.
- [12] R. Verzicco, M. Fatica, G. Iaccarino, P. Moin, and B. Khalighi, "Large Eddy Simulation of a Road Vehicle with Drag-Reduction Devices," *AIAA Journal*, vol. 40, no. 12, pp. 2447–2455, 2002.
- [13] J. D. Coon and K. D. Visser, "Drag Reduction of a Tractor-Trailer Using Planar," *The Aerodynamic of Heavy Vehicles: Trucks, Buses, and Trains*, vol. 1, 2004.
- [14] S. Krajnović, "Large Eddy Simulation Exploration of Passive Flow Control Around an Ahmed Body," *Journal of Fluids Engineering*, vol. 136, p. 121103, sep 2014.
- [15] V. J. Modi and V. S. Deshpande, "Fluid dynamics of a cubic structure as affected by momentum injection and height," *Journal of Wind Engineering and Industrial Aerodynamics*, vol. 89, no. 5, pp. 445–470, 2001.

- [16] X. Han and S. Krajnović, “Large Eddy Simulation of Flow Control Around a Cube Subjected to Momentum Injection,” *Journal of Fluid Mechanics*, vol. 729, pp. 151–179, apr 2013.
- [17] E. Moreau, “Airflow control by non-thermal plasma actuators,” *Journal of Physics D: Applied Physics*, vol. 40, no. 3, pp. 605–636, 2007.
- [18] T. C. Corke, C. L. Enloe, and S. P. Wilkinson, “Dielectric Barrier Discharge Plasma Actuators for Flow Control\*,” *Annual Review of Fluid Mechanics*, vol. 42, no. 1, pp. 505–529, 2010.
- [19] N. Benard and E. Moreau, “Electrical and mechanical characteristics of surface AC dielectric barrier discharge plasma actuators applied to airflow control,” *Experiments in Fluids*, vol. 55, no. 11, 2014.
- [20] J. R. Roth, D. M. Sherman, and S. P. Wilkinson, “Boundary layer flow control with a one atmosphere uniform glow discharge surface plasma,” *36th Aerospace Sciences Meeting & Exhibit January*, vol. 28, 1998.
- [21] R. E. Hanson, P. Lavoie, A. M. Naguib, and J. F. Morrison, “Transient growth instability cancelation by a plasma actuator array,” *Experiments in Fluids*, vol. 49, no. 6, pp. 1339–1348, 2010.
- [22] S. Krajnović, J. Östh, and B. Basara, “LES study of breakdown control of A-pillar vortex,” *International Journal of Flow Control*, vol. 2, pp. 237–258, dec 2010.
- [23] M. Amitay and A. Glezer, “Role of Actuation Frequency in Controlled Flow Reattachment over a Stalled Airfoil,” *AIAA Journal*, vol. 40, pp. 209–216, feb 2002.
- [24] D. You and P. Moin, “Active control of flow separation over an airfoil using synthetic jets,” *Journal of Fluids and Structures*, vol. 24, pp. 1349–1357, nov 2008.
- [25] A. Brunn and W. Nitsche, “Active control of turbulent separated flows over slanted surfaces,” *International Journal of Heat and Fluid Flow*, vol. 27, pp. 748–755, oct 2006.
- [26] S. Krajnović and J. Fernandes, “Numerical simulation of the flow around a simplified vehicle model with active flow control,” *International Journal of Heat and Fluid Flow*, vol. 32, pp. 192–200, feb 2011.
- [27] L. N. Cattafesta and M. Sheplak, “Actuators for Active Flow Control,” *Annual Review of Fluid Mechanics*, vol. 43, pp. 247–272, jan 2011.
- [28] S. L. Brunton and B. R. Noack, “Closed-Loop Turbulence Control: Progress and Challenges,” *Applied Mechanics Reviews*, vol. 67, no. 5, p. 050801, 2015.
- [29] A. Siefert, T. Bachar, D. Koss, M. Shephelovich, and I. Wygnanski, “Oscillatory blowing: A tool to delay boundary-layer separation,” *AIAA journal*, vol. 31, no. 11, pp. 2052–2060, 1993.
- [30] J.-Z. Wu, X.-Y. Lu, A. G. Denny, M. Fan, and J.-M. Wu, “Post-stall flow control on an airfoil by local unsteady forcing,” *Journal of Fluid Mechanics*, vol. 371, pp. 21–58, 1998.
- [31] A. Glezer, M. Amitay, and A. M. Honohan, “Aspects of Low- and High-Frequency Actuation for Aerodynamic Flow Control,” *AIAA Journal*, vol. 43, no. 7, pp. 1501–1511, 2005.

- [32] M. F. Unal and D. Rockwell, “On vortex formation from a cylinder. Part 1. The initial instability,” *Journal of Fluid Mechanics*, vol. 190, pp. 491–512, 1988.
- [33] S. B. Pope, *Turbulent Flows*, vol. 12. 2001.
- [34] O. Reynolds, “On the dynamical theory of incompressible viscous fluids and the determination of the criterion,” *Philos. Trans. R. Soc. London*, vol. 186, pp. 123–164.
- [35] S. Kurien and M. a. Taylor, “Direct Numerical Simulations of Turbulence Data Generation and Statistical Analysis,” *Los A*, no. 29, pp. 142–151, 2005.
- [36] T. Ishihara, T. Gotoh, and Y. Kaneda, “Study of high-Reynolds number isotropic turbulence by direct numerical simulation,” *Annual Review of Fluid Mechanics*, vol. 41, no. 1, pp. 165–180, 2009.
- [37] T. Ishihara, Y. Kaneda, M. Yokokawa, K. Itakura, and A. Uno, “Small-scale statistics in high-resolution direct numerical simulation of turbulence: Reynolds number dependence of one-point velocity gradient statistics,” *Journal of Fluid Mechanics*, vol. 592, pp. 335–366, 2007.
- [38] P. Schlatter and R. Örlü, “Assessment of direct numerical simulation data of turbulent boundary layers,” *Journal of Fluid Mechanics*, vol. 659, pp. 116–126, 2010.
- [39] J. Ahn, J. H. Lee, J.-h. Kang, and H. J. Sung, “Direct numerical simulation of a 30R long turbulent pipe flow at  $R^+ = 685$ : large- and very large-scale motions,” *Physics of Fluids*, vol. 27, p. 065110, 2015.
- [40] J. Boussinesq, “Essai sur la théorie des eaux courantes,” *Imprimerie nationale*, vol. 2, 1877.
- [41] M. El-Alti, *Active Flow Control for Drag Reduction of Heavy Vehicles*. Doktorsavhandlingar vid Chalmers tekniska högskola. Ny serie, no: 3452, Department of Applied Mechanics, Fluid Dynamics, Chalmers University of Technology,, 2012.
- [42] H. Hafsteinsson, *Study of Supersonic Jet Noise Reduction using LES*. Doktorsavhandlingar vid Chalmers tekniska högskola. Ny serie, no: 3767, Department of Applied Mechanics, Fluid Dynamics, Chalmers University of Technology,, 2014.
- [43] J. Östh, *Unsteady Numerical Simulations and Reduced-Order Modelling of Flows around Vehicles*. Doktorsavhandlingar vid Chalmers tekniska högskola. Ny serie, no:, Department of Applied Mechanics, Fluid Dynamics, Chalmers University of Technology,, 2014.
- [44] J. Smagorinsky, “General circulation experiments with the primitive equations,” *Monthly weather review*, vol. 91 (3), pp. 99–165, 1963.
- [45] S. Krajnovic, *Large-Eddy Simulations for Computing the Flow Around Vehicles*. Department of Thermo and Fluid Dynamics, Chalmers University of Technology,, 2002.
- [46] H. Hemida, *Numerical Simulations of Flows around Trains and Buses in Cross Winds*. Doktorsavhandlingar vid Chalmers tekniska högskola. Ny serie, no: 2868, Department of Applied Mechanics, Fluid Dynamics, Chalmers University of Technology,, 2008.
- [47] H. Choi and P. Moin, “Grid-point requirements for large eddy simulation: Chapman’s estimates revisited,” *Physics of Fluids*, vol. 24, no. 1, pp. 13–18, 2012.

- [48] U. Piomelli and E. Balaras, “Wall-Layer Models for Large Eddy Simulations,” *Annual Review of Fluid Mechanics*, vol. 34, pp. 349–374, 2002.
- [49] P. R. Spalart, W. H. Jou, M. Strelets, and S. R. Allmaras, “Comments on the feasibility of LES for wings and on a hybrid RANS/LES approach,” in *Proceedings of the First AFOSR International Conference on DNS/LES*, vol. 1, pp. 137–147, 1997.
- [50] B. Nebenführ, *Turbulence-resolving simulations for engineering applications*. Department of Applied Mechanics, Fluid Dynamics, Chalmers University of Technology, 2015.
- [51] P. R. Spalart, S. Deck, M. L. Shur, K. D. Squires, M. K. Strelets, and A. Travin, “A new version of detached-eddy simulation, resistant to ambiguous grid densities,” *Theoretical and Computational Fluid Dynamics*, vol. 20, no. 3, pp. 181–195, 2006.
- [52] L. Davidson and S. H. Peng, “Hybrid LES-RANS modelling: A one-equation SGS model combined with a k-w model for predicting recirculating flows,” *International Journal for Numerical Methods in Fluids*, vol. 43, no. 9, pp. 1003–1018, 2003.
- [53] S. H. Peng, “Hybrid RANS-LES modeling based on zero- and one-equation models for turbulent flow simulation,” in *4th International Symposium on Turbulence and Shear Flow Phenomena*, vol. 3, pp. 1159–1164, 2005.
- [54] S. S. Girimaji, E. Jeong, and R. Srinivasan, “Partially Averaged Navier-Stokes Method for Turbulence: Fixed Point Analysis and Comparison With Unsteady Partially Averaged Navier-Stokes,” *Journal of Applied Mechanics*, vol. 73, no. 3, p. 422, 2006.
- [55] S. S. Girimaji, “Partially-Averaged Navier-Stokes Model for Turbulence: A Reynolds-Averaged Navier-Stokes to Direct Numerical Simulation Bridging Method,” *Journal of Applied Mechanics*, vol. 73, no. 3, p. 413, 2006.
- [56] E. Jeong and S. S. Girimaji, “Partially Averaged Navier–Stokes (PANS) Method for Turbulence Simulations—Flow Past a Square Cylinder,” *Journal of Fluids Engineering*, vol. 132, no. 12, p. 121203, 2010.
- [57] S. Lakshminpathy and S. S. Girimaji, “Partially Averaged Navier–Stokes (PANS) Method for Turbulence Simulations: Flow Past a Circular Cylinder,” *Journal of Fluids Engineering*, vol. 132, no. 12, p. 121202, 2010.
- [58] S. Lakshminpathy and S. Girimaji, “Partially-averaged Navier-Stokes method for turbulent flows: k-w model implementation,” in *44th AIAA Aerospace Sciences Meeting and Exhibit*, Aerospace Sciences Meetings, American Institute of Aeronautics and Astronautics, jan 2006.
- [59] J. M. Ma, S. H. Peng, L. Davidson, and F. J. Wang, “A low Reynolds number variant of partially-averaged Navier-Stokes model for turbulence,” *International Journal of Heat and Fluid Flow*, vol. 32, no. 3, pp. 652–669, 2011.
- [60] P. A. Durbin, “Near-wall turbulence closure modeling without ”damping functions”,” *Theoretical and Computational Fluid Dynamics*, vol. 3, no. 1, pp. 1–13, 1991.
- [61] K. Hanjalić, M. Popovac, and M. Hadžiabdić, “A robust near-wall elliptic-relaxation eddy-viscosity turbulence model for CFD,” *International Journal of Heat and Fluid Flow*, vol. 25, pp. 1047–1051, dec 2004.

- [62] B. Basara, S. Krajnović, and S. Girimaji, “PANS methodology applied to elliptic-relaxation based eddy viscosity transport model,” *Turbulence and Interactions*, pp. 63–69, 2010.
- [63] B. Basara, S. Krajnovic, S. Girimaji, and Z. Pavlovic, “Near-Wall Formulation of the Partially Averaged Navier Stokes Turbulence Model,” *AIAA Journal*, vol. 49, pp. 2627–2636, dec 2011.
- [64] S. Krajnović, R. Lárusson, and B. Basara, “Superiority of PANS compared to LES in predicting a rudimentary landing gear flow with affordable meshes,” *International Journal of Heat and Fluid Flow*, vol. 37, pp. 109–122, oct 2012.
- [65] S. Krajnović, G. Minelli, and B. Basara, “Partially-averaged Navier-Stokes simulations of two bluff body flows,” *Applied Mathematics and Computation*, vol. 000, pp. 1–15, 2015.
- [66] S. Krajnović and G. Minelli, “Status of PANS for bluff body aerodynamics of engineering relevance,” *Notes on Numerical Fluid Mechanics and Multidisciplinary Design*, vol. 130, pp. 399–410, 2015.
- [67] S. Krajnović, G. Minelli, and B. Basara, “Partially-Averaged Navier-Stokes Simulations of Flows Around Generic Vehicle at Yaw,” *SAE Technical Paper*, 2016.
- [68] M. Germano, “Turbulence: the filtering approach,” *Journal of Fluid Mechanics*, vol. 238, pp. 325–336, 1992.
- [69] S. S. Girimaji, “Partially-Averaged Navier-Stokes Model for Turbulence: A Reynolds-Averaged Navier-Stokes to Direct Numerical Simulation Bridging Method,” *Journal of Applied Mechanics*, vol. 73, no. 3, p. 413, 2006.
- [70] S. Girimaji and K. Abdol-Hamid, “Partially Averaged Navier–Stokes Model for Turbulence: Implementation and Validation,” *AIAA paper*, no. January, 2005.
- [71] D. D. Kosambi, “Statistics in Function Space,” *The Journal of the Indian Mathematical Society*, vol. 7, pp. 76–88, 1943.
- [72] J. L. Lumley, “The Structure of Inhomogeneous Turbulent Flows,” in *Atmospheric turbulence and radio propagation* (A. M. Yaglom and V. I. Tatarski, eds.), pp. 166–178, Moscow: Nauka, 1967.
- [73] P. Holmes, J. L. Lumley, G. B. Thomson, and C. W. Rowley, “Turbulence, coherent structures, dynamical systems and symmetry,” *Cambridge University press*, p. 2500, 1997.
- [74] P. Schmid, “Dynamic mode decomposition of numerical and experimental data,” *Journal of Fluid Mechanics*, vol. 656, pp. 5–28, jul 2010.
- [75] P. J. Schmid, L. Li, M. P. Juniper, and O. Pust, “Applications of the dynamic mode decomposition,” *Theoretical and Computational Fluid Dynamics*, vol. 25, pp. 249–259, aug 2011.
- [76] J. Tu, C. Rowley, E. Aram, and R. Mittal, “Koopman spectral analysis of separated flow over a finite-thickness flat plate with elliptical leading edge,” *AIAA Paper 2011*, no. January, pp. 1–14, 2011.
- [77] T. W. Muld, G. Efraimsson, and D. S. Henningson, “Flow structures around a high-speed train extracted using Proper Orthogonal Decomposition and Dynamic Mode Decomposition,” *Computers and Fluids*, vol. 57, pp. 87–97, mar 2012.

- [78] J. Östh, B. R. Noack, S. Krajnović, D. Barros, and J. Borée, “On the need for a nonlinear subscale turbulence term in POD models as exemplified for a high Reynolds number flow over an Ahmed body,” *Journal of Fluid Mechanics*, pp. 1–26, oct 2013.
- [79] J. Östh, E. Kaiser, S. Krajnović, and B. R. Noack, “Cluster-based reduced-order modelling of the flow in the wake of a high speed train,” *Journal of Wind Engineering and Industrial Aerodynamics*, vol. 145, pp. 327–338, 2015.
- [80] J. L. Lumley, *Stochastic Tools in Turbulence - Applied Mathematics and Mechanics*, vol. 12. New York: Academic Press, 1970.
- [81] D. Rempfer and H. F. Fasel, “Evolution of three-dimensional coherent structures in a flat-plate boundary layer,” *Journal of Fluid Mechanics*, vol. 260, no. -1, p. 351, 1994.